LA-UR- 00-5289

Approved for public release; distribution is unlimited.

Title: **EXACT SOLUTION OF HEAT CONDUCTION IN A TWO-DOMAIN COMPOSITE CYLINDER WITH AN ORTHOTROPIC OUTER LAYER**

Author(s): **C. Aviles-Ramos and C. R. Rudy**

Submitted to: **35th National Heat Transfer Conference
Anaheim, CA
June 10-12, 2001
(FULL PAPER)**

Los Alamos
NATIONAL LABORATORY

DISCLAIMER

DISCLAIMER

Portions of this document may be illegible in electronic image products. Images are produced from the best available original document.

Exact Solution of Heat Conduction in a Two-Domain Composite Cylinder with an Orthotropic Outer Layer

C. A. Ramos, and C. Rudy
Los Alamos National Laboratory
NIS-5 Safeguards Science and Technology
Los Alamos, New Mexico 87545

ABSTRACT

The transient exact solution of heat conduction in a two-domain composite cylinder is developed using the separation of variables technique. The inner cylinder is isotropic and the outer cylindrical layer is orthotropic. Temperature solutions are obtained for boundary conditions of the first and second kinds at the outer surface of the orthotropic layer. These solutions are applied to heat flow calorimeters modeling assuming that there is heat generation due to nuclear reactions in the inner cylinder. Heat flow calorimeter simulations are carried out assuming that the inner cylinder is filled with plutonium oxide powder. The first objective in these simulations is to predict the onset of thermal equilibrium of the calorimeter with its environment. Two types of boundary conditions at the outer surface of the orthotropic layer are used to predict thermal equilibrium. The procedure developed to carry out these simulations can be used as a guideline for the design of calorimeters.

Another important application of these solutions is on the estimation of thermophysical properties of orthotropic cylinders. The thermal conductivities in the vertical, radial and circumferential directions of the orthotropic outer layer can be estimated using this exact solution and experimental data. Simultaneous estimation of the volumetric heat capacity and thermal conductivities is also possible. Furthermore, this

solution has potential applications to the solution of the inverse heat conduction problem in this cylindrical geometry.

An interesting feature of the construction of this solution is that two different sets of eigenfunctions need to be considered in the eigenfunction expansion. These eigenfunctions sets depend on the relative values of the thermal diffusivity of the inner cylinder and the thermal diffusivity in the vertical direction of the outer cylindrical layer.

Nomenclature

a,b,d	dimensions in Fig. 1, *cm*
$\bar{a}$	$a\sqrt{k_{z2}/k_{r2}}$
A_0	$2\pi b d$
A_d	πa^2
A_{mn}	Fourier coefficients, Eqs. (14) or (15)
$\bar{b}$	$b\sqrt{k_{z2}/k_{r2}}$
c_{p1}	heat capacity of region 1, *J/kgK*
c_{p2}	heat capacity of region 2, *J/kgK*
C_{mn}	coefficients, Eqs. (17) and (28)
C^{*}_{mn}	coefficients, Eqs. (21) and (30)
C^{**}_{mn}	coefficients, Eqs. (25) and (32)
D_{mn}	coefficients, Eqs. (17) and (29)
D^{*}_{mn}	coefficients, Eqs. (21) and (31)
D^{**}_{mn}	coefficients, Eqs. (25) and (33)
f_1	initial condition in region 1
f_2	initial condition in region 2
$F_{1,mn}$	eigenfunction, Eq. (16)
$F_{2,mn}$	eigenfunction, Eq. (17)
$F^{*}_{1,mn}$	eigenfunction, Eq. (20)

$F^{*}_{2,mn}$ eigenfunction, Eq. (21)

$F^{**}_{1,mn}$ eigenfunction, Eq. (24)

$F^{**}_{2,mn}$ eigenfunction, Eq. (25)

g_i volumetric heat source, W/cm^3

h heat transfer coefficient, $W/(cm^2\ ^\circ C)$

i index

I_0 modified Bessel function of the first kind and order zero

J_0 Bessel function of the first kind and order zero

K_0 modified Bessel function of the second kind and order zero

k_{r2} thermal conductivity in region 2 along r-direction, W/cmK

k_{z2} thermal conductivity in region 2 along z-direction, W/cmK

k_1 thermal conductivity in region 1, W/cmK

k $\sqrt{k_{z2}/k_{r2}}$

m,n indices in eigenfunctions

N_{mn} norm, Eq. (40)

N^{*}_{mn} norm, Eq. (41)

N^{**}_{mn} norm, Eq. (42)

P upper limit of summation, Eq. (86)

$q(t)$ heat flux function, Eq. (86), W/cm^2

q_0 heat flux at $r=b$, Eq. (7), W/cm^2

q_{z1} heat flux at $z=0$, Eq. (4), W/cm^2

q_{z2} heat flux at $z=d$, Eq. (5), W/cm^2

t time, s

T_∞ environmental temperature, $^\circ C$

T_i temperature in regions 1 or 2, $^\circ C$

T_s prescribed surface temperature, $^\circ C$

V_0 volume of region 1, cm^3

$\bar{r}$ $r\sqrt{k_{z2}/k_{r2}}$

r coordinate, cm

Y_0 Bessel function of the second kind and order zero

z coordinate, cm

Greek

α_{z2} thermal diffusivity in region 2, in z-direction, cm^2/s

α_1 thermal diffusivity in region 1, cm^2/s

δ Dirac delta function

γ_{mn} eigenvalue for the r-direction in region 2, Eq. (18), cm^{-1}

γ^*_{mn} eigenvalue for the r-direction in region 2, Eq. (22), cm^{-1}

γ^{**}_{mn} eigenvalue for the r-direction in region 2, Eq. (26), cm^{-1}

η_{mn} eigenvalue for the r-direction in region 1, Eq. (19), cm^{-1}

η^*_{mn} eigenvalue for the r-direction in region 1, Eq. (23), cm^{-1}

η^{**}_{mn} eigenvalue for the r-direction in region 1, Eq. (27), cm^{-1}

λ_{mn} eigenvalue for time, s^{-1}

λ^*_{mn} eigenvalue for time, s^{-1}

λ^{**}_{mn} eigenvalue for time, s^{-1}

Λ_{mn} initial condition constant, Eq. (49)

Λ^*_{mn} initial condition constant, Eq. (50)

Λ^{**}_{mn} initial condition constant, Eq. (51)

μ, ν indices

ρ_1, ρ_2 density of regions 1 and 2, kg/cm^3

ξ integer function

Introduction

This solution was originally developed as a result of the need for a thermal model for a calorimeter experimental set-up intended to measure the power generated by 5 gallons drums of enriched uranium or plutonium. The research on this experimental set-up will

lead to the development of a calorimeter capable of measuring the power from 55-gallon shipping containers. Also, this calorimeter will be capable of measuring uranium contents of objects such as fuel plates, weapons components, and other uranium processes materials. The geometry of the solution presented here was selected as the most simplified form of the calorimeter thermal model. It is assumed that the inner cylinder constitutes the nuclear material and that the outer cylinder is a power sensor that measures a bridge potential between the inner and outer surfaces of the outer cylinder. The outer cylinder is assumed to be orthotropic because of the geometrical distribution of the materials that compose this power sensor.

This paper discusses the procedure of the application of the separation of variables technique to a system of two partial differential equations which govern the heat conduction in a two-domain cylindrical geometry. An important part in the construction of this solution is the calculation of the eigenvalues. The eigenvalues are calculated applying the boundary conditions at the outer surface, and the continuity of the temperature and heat flux at the interface between the two cylindrical domains. Two sets of eigenfunctions are defined for the construction of this solution. One eigenfunction set applies for the case where $\alpha_1 > \alpha_{z2}$ and another set applies when $\alpha_1 < \alpha_{z2}$.

Analysis

The heat conduction equation in the isotropic inner cylinder is

$$k_1 \frac{1}{r}\frac{\partial}{\partial r}\left(r\frac{\partial T_1}{\partial r}\right) + k_1 \frac{\partial^2 T_1}{\partial z^2} + g_1(r,z,t) = \rho_1 c_{p1}\frac{\partial T_1}{\partial t} \quad \text{in} \quad 0 < r < a \tag{1}$$

Also, the diffusion equation in orthotropic outer layer has the form

$$k_{r2} \frac{1}{r}\frac{\partial}{\partial r}\left(r\frac{\partial T_2}{\partial r}\right) + k_{z2} \frac{\partial^2 T_2}{\partial z^2} + g_2(r,z,t) = \rho_2 c_{p2}\frac{\partial T_2}{\partial t} \quad \text{in } a < r < b \tag{2}$$

where $g_1(r,z,t)$ and $g_2(r,z,t)$ are volumetric heat source functions. The volumetric heat generation function $g_2(r,z,t)$ could include the heat flux at the surface $r = b$. Subscripts

1 and 2 indicate the inner and outer cylinders respectively. The solutions of Eqs. (1) and (2) are sought for the following boundary and initial conditions

$$\frac{\partial T_1}{\partial r} = 0 \quad \text{at} \quad r = 0 \tag{3}$$

$$k_1 \frac{\partial T_1}{\partial z} = q_{z1}(r,t) \quad \text{at } z = 0 \text{ in } 0 < r < a \tag{4}$$

$$k_1 \frac{\partial T_1}{\partial z} = q_{z2}(r,t) \quad \text{at } z = d \text{ in } 0 < r < a \tag{5}$$

$$k_{z2} \frac{\partial T_2}{\partial z} = 0 \quad \text{at } z = 0 \text{ and } z = d \text{ in } a < r < b \tag{6}$$

$$k_{r2} \frac{\partial T_2}{\partial r} = q_0(z,t) \text{ at } r = b \text{ in } 0 < z < d \tag{7}$$

$$T_1(r,z,0) = f_1(r,z) \text{ and } T_2(r,z,0) = f_2(r,z) \tag{8}$$

To make the presentation of this solution more compact, the top and bottom surfaces of the outer cylindrical layer are assumed to be insulated. An additional solution for prescribed temperature at the surface $r = b$ is also constructed by replacing Eq. (7) with the boundary condition

$$T_2(b,z,t) = T_s(z,t) \text{ in } 0 < z < d \tag{9}$$

The solution is obtained applying a standard transformation in the r direction as

$$\bar{r} = \sqrt{\frac{k_{z2}}{k_{r2}}}\, r \tag{10}$$

Equation (10) transforms the heat conduction equation in region 2 as

$$\frac{1}{\bar{r}} \frac{\partial}{\partial \bar{r}} \left(\bar{r} \frac{\partial T_2}{\partial \bar{r}} \right) + \frac{\partial^2 T_2}{\partial z^2} + \frac{g_2(\bar{r},z,t)}{k_{z2}} = \frac{1}{\alpha_{z2}} \frac{\partial T_2}{\partial t} \text{ in } \bar{a} < r < \bar{b} \tag{11}$$

The compatibility conditions at the interface $r = a$ are taken as

$$T_1(a,z,t) = T_2(a,z,t) \tag{12}$$

$$k_1 \frac{\partial T_1}{\partial r} = k_{r2} \frac{\partial T_2}{\partial r} \quad \text{at } r = a \tag{13}$$

The separation of variables technique applied to the homogeneous forms of Eqs. (1) and (11) produces two eigenfunction expansions with the form

$$T_i(r,z,t)=\sum_{m=0}^{\infty}\sum_{n=0}^{\infty}A_{mn}(t)\,F_{i,mn}(r,z)\exp\left(-\lambda_{mn}^2\,t\right)$$
$$+\sum_{m=1}^{\xi(n)}\sum_{n=1}^{\infty}A_{mn}^{*}(t)\,F_{i,mn}^{*}(r,z)\exp\left(-\lambda_{mn}^{*2}\,t\right)\ \text{for } i=1,2\ \text{ and }\ \alpha_1<\alpha_{z2} \tag{14}$$

$$T_i(r,z,t)=\sum_{m=0}^{\infty}\sum_{n=0}^{\infty}A_{mn}(t)\,F_{i,mn}(r,z)\exp\left(-\lambda_{mn}^2\,t\right)$$
$$+\sum_{m=1}^{\xi(n)}\sum_{n=1}^{\infty}A_{mn}^{**}(t)\,F_{i,mn}^{**}(r,z)\exp\left(-\lambda_{mn}^{**2}\,t\right)\ \text{for } i=1,2\ \text{ and }\ \alpha_1>\alpha_{z2} \tag{15}$$

the eigenfunctions $F_{i,mn}(r,z)$ for $i=1,2$ are defined as

$$F_{1,mn}(r,z)=J_0(\eta_{mn}r)\cos(n\pi\,z/d) \tag{16}$$

$$F_{2,mn}(r,z)=\left[C_{mn}\,J_0(\gamma_{mn}kr)+D_{mn}Y_0(\gamma_{mn}kr)\right]\cos(n\pi\,z/d) \tag{17}$$

where $k=\sqrt{k_{z2}/k_{r2}}$, J_0 and Y_0 are the zero order Bessel's functions of the first and second kinds respectively, γ_{mn} and η_{mn} are related to λ_{mn} by the equations

$$\gamma_{mn}=\sqrt{\lambda_{mn}^2/\alpha_{z2}-(n\pi/d)^2} \tag{18}$$

$$\eta_{mn}=\sqrt{\lambda_{mn}^2/\alpha_1-(n\pi/d)^2} \tag{19}$$

in which $\alpha_{z2}=\rho_2c_{p2}/k_{z2}$ and $\alpha_1=\rho_1c_{p1}/k_1$. The upper limit, $\xi(n)$, of the summations appearing in Eqs. (14) and (15) is an integer function that depends on the number of eigenvalues present for each specified value of n. The eigenvalues $\sqrt{\lambda_{mn}^2/\alpha_{z2}-(n\pi/d)^2}$ and $\sqrt{\lambda_{mn}^2/\alpha_1-(n\pi/d)^2}$ can be real or imaginary depending on the relative values of α_{z2} and α_1. When $\alpha_1<\alpha_{z2}$ $\sqrt{\lambda_{mn}^2/\alpha_{z2}-(n\pi/d)^2}$ can be real or complex while $\sqrt{\lambda_{mn}^2/\alpha_1-(n\pi/d)^2}$ takes over real values only. For the case when $\alpha_1>\alpha_{z2}$, $\sqrt{\lambda_{mn}^2/\alpha_1-(n\pi/d)^2}$ can be real or imaginary while $\sqrt{\lambda_{mn}^2/\alpha_{z2}-(n\pi/d)^2}$ assumes real values only. This results in two different sets of eigenfunctions to be used in the construction of the solution. The eigenfunctions appearing in the second terms of Eqs. (14) and (15) make these eigenfunctions sets different. For the case where $\alpha_1<\alpha_{z2}$ the eigenfunctions, $F_{i,mn}^{*}(r,z)$ for $i=1,2$; have the form

$$F_{1,mn}^{*}(r,z)=J_0(\eta_{mn}^{*}r)\cos(n\pi\,z/d) \tag{20}$$

$$F_{2,mn}^{*}(r,z)=\left[C_{mn}^{*}\,I_0(\gamma_{mn}^{*}kr)+D_{mn}^{*}K_0(\gamma_{mn}^{*}kr)\right]\cos(n\pi\,z/d) \tag{21}$$

in which I_0 and K_0 are zero order modified Bessel's functions of the first and second kind respectively. The eigenvlaues η^*_{mn} and γ^*_{mn} are related to λ^*_{mn} through the equations

$$\gamma^*_{mn} = \sqrt{(n\pi/d)^2 - \lambda^{*2}_{mn}/\alpha_{z2}} \tag{22}$$

$$\eta^*_{mn} = \sqrt{\lambda^{*2}_{mn}/\alpha_1 - (n\pi/d)^2} \tag{23}$$

The eigenfunctions appearing in the second term of Eq. (15) apply when $\alpha_1 > \alpha_{z2}$ and are given by

$$F^{**}_{1,mn}(r,z) = I_0(\eta^{**}_{mn} r)\cos(n\pi z/d) \tag{24}$$

$$F^{**}_{2,mn}(r,z) = \left[C^{**}_{mn} J_0(\gamma^{**}_{mn} kr) + D^{**}_{mn} Y_0(\gamma^{**}_{mn} kr)\right]\cos(n\pi z/d) \tag{25}$$

where η^{**}_{mn} and γ^{**}_{mn} are related to λ^{**}_{mn} by the equations

$$\gamma^{**}_{mn} = \sqrt{\lambda^{**2}_{mn}/\alpha_{z2} - (n\pi/d)^2} \tag{26}$$

$$\eta^{**}_{mn} = \sqrt{(n\pi/d)^2 - \lambda^{**2}_{mn}/\alpha_1} \tag{27}$$

The contact conditions at the interface $r = a$, Eqs. (12) and (13), yield the constants C_{mn}, D_{mn}, C^*_{mn}, D^*_{mn}, C^{**}_{mn}, and D^{**}_{mn} appearing in Eqs. (17), (21) and (25) as

$$C_{mn} = -\pi\gamma_{mn}\bar{a}J_0(\eta_{mn}a)Y_1(\gamma_{mn}\bar{a})/2 + \pi\eta_{mn}k_1 a J_1(\eta_{mn}a)Y_0(\gamma_{mn}\bar{a})/(2k_{r2}) \tag{28}$$

$$D_{mn} = \pi\gamma_{mn}\bar{a}J_0(\eta_{mn}a)J_1(\gamma_{mn}\bar{a})/2 - \pi\eta_{mn}k_1 a J_1(\eta_{mn}a)J_0(\gamma_{mn}\bar{a})/(2k_{r2}) \tag{29}$$

$$C^*_{mn} = \gamma^*_{mn}\bar{a}J_0(\eta^*_{mn}a)K_1(\gamma^*_{mn}\bar{a}) + \eta^*_{mn}k_1\bar{a}J_1(\eta^*_{mn}a)K_0(\gamma^*_{mn}\bar{a})/\sqrt{k_{r2}k_{z2}} \tag{30}$$

$$D^*_{mn} = \gamma^*_{mn}\bar{a}J_0(\eta^*_{mn}a)I_1(\gamma^*_{mn}\bar{a}) - \eta_{mn}k_1\bar{a}J_1(\eta^*_{mn}a)I_0(\gamma^*_{mn}\bar{a})/\sqrt{k_{r2}k_{z2}} \tag{31}$$

$$C^{**}_{mn} = -\pi\gamma_{mn}\bar{a}I_0(\eta^{**}_{mn}a)Y_1(\gamma^{**}_{mn}\bar{a})/2 - \pi\eta^{**}_{mn}k_1 a I_1(\eta^{**}_{mn}a)Y_0(\gamma^{**}_{mn}\bar{a})/(2k_{r2}) \tag{32}$$

$$D^{**}_{mn} = \pi\gamma_{mn}\bar{a}I_0(\eta^{**}_{mn}a)J_1(\gamma^{**}_{mn}\bar{a})/2 + \pi\eta^{**}_{mn}k_1 a I_1(\eta^{**}_{mn}a)J_0(\gamma^{**}_{mn}\bar{a})/(2k_{r2}) \tag{33}$$

The homogeneous form of boundary condition (7) yields the transcendental equations for the estimation of the eigenvalues λ_{mn}, λ^*_{mn}, and λ^{**}_{mn}. The transcendental equation that produces the eigenvalues λ_{mn} applies for $\alpha_1 < \alpha_{z2}$ or $\alpha_1 > \alpha_{z2}$ and has the form

$$C_{mn}/D_{mn} = -Y_1(\gamma_{mn}\bar{b})/J_1(\gamma_{mn}\bar{b}) \tag{34}$$

The case $\alpha_1 < \alpha_{z2}$ produces the transcendental equation

$$C^*_{mn}/D^*_{mn} = -K_1(\gamma^*_{mn}\bar{b})/I_1(\gamma^*_{mn}\bar{b}) \tag{35}$$

which is used to calculate the eigenvalues λ^{*}_{mn}. When $\alpha_1 > \alpha_{z2}$ the transcendental equation

$$C^{**}_{mn} / D^{**}_{mn} = -Y_1(\gamma^{**}_{mn}\bar{b}) / J_1(\gamma^{**}_{mn}\bar{b}) \tag{36}$$

produces the eigenvalues λ^{**}_{mn}. The eigenvalues obtained from Eqs. (34) and (35) are used to construct the solution given by Eq. (14) while the eigenvalues obtained from Eqs. (34) and (36) are used to generate the eigenfunction expansion (15).

Orthogonality. An orthogonality study showed that

$$(\lambda^{2}_{\mu\nu} - \lambda^{2}_{mn})\left[\int_{r=0}^{a}\int_{z=0}^{d} \rho_1 c_{p1} F_{1,\mu\nu} F_{1,mn} r dr dz + \int_{r=a}^{b}\int_{z=0}^{d} \rho_2 c_{p2} F_{2,\mu\nu} F_{2,mn} r dr dz\right] = 0 \tag{37}$$

$$(\lambda^{*2}_{\mu\nu} - \lambda^{*2}_{mn})\left[\int_{r=0}^{a}\int_{z=0}^{d} \rho_1 c_{p1} F^{*}_{1,\mu\nu} F^{*}_{1,mn} r dr dz + \int_{r=a}^{b}\int_{z=0}^{d} \rho_2 c_{p2} F^{*}_{2,\mu\nu} F^{*}_{2,mn} r dr dz\right] = 0 \tag{38}$$

$$(\lambda^{**2}_{\mu\nu} - \lambda^{**2}_{mn})\left[\int_{r=0}^{a}\int_{z=0}^{d} \rho_1 c_{p1} F^{**}_{1,\mu\nu} F^{**}_{1,mn} r dr dz + \int_{r=a}^{b}\int_{z=0}^{d} \rho_2 c_{p2} F^{**}_{2,\mu\nu} F^{**}_{2,mn} r dr dz\right] = 0 \tag{39}$$

The term between square brackets in Eqs. (37), (38), and (39) is equal to zero except when $\mu = m$ and $\nu = n$. Therefore the norms are

$$N_{mn} = \int_{r=0}^{a}\int_{z=0}^{d} \rho_1 c_{p1} \left(F_{1,mn}\right)^2 r dr dz + \int_{r=a}^{b}\int_{z=0}^{d} \rho_2 c_{p2} \left(F_{2,mn}\right)^2 r dr dz \tag{40}$$

$$N^{*}_{mn} = \int_{r=0}^{a}\int_{z=0}^{d} \rho_1 c_{p1} \left(F^{*}_{1,mn}\right)^2 r dr dz + \int_{r=a}^{b}\int_{z=0}^{d} \rho_2 c_{p2} \left(F^{*}_{2,mn}\right)^2 r dr dz \tag{41}$$

$$N^{**}_{mn} = \int_{r=0}^{a}\int_{z=0}^{d} \rho_1 c_{p1} \left(F^{**}_{1,mn}\right)^2 r dr dz + \int_{r=a}^{b}\int_{z=0}^{d} \rho_2 c_{p2} \left(F^{**}_{2,mn}\right)^2 r dr dz \tag{42}$$

Temperature Solutions. The temperature solutions are obtained substituting Eqs. (14) and (15) into Eqs. (1) and (2), and making use of the two-dimensional eigenvalue problem and the orthogonality conditions (37), (38), and (39) to obtain

$$\frac{dA_{mn}}{dt} = \frac{1}{N_{mn}}\left[\int_{r=0}^{a}\int_{z=0}^{d} \rho_1 c_{p1} g_1(r,z,t) F_{1,mn}(r,z) r dr dz + \int_{r=a}^{b}\int_{z=0}^{d} \rho_2 c_{p2} g_2(r,z,t) F_{2,mn}(r,z) r dr dz\right] \exp\left(\lambda^{2}_{mn} t\right) \tag{43}$$

$$\frac{dA^{*}_{mn}}{dt} = \frac{1}{N^{*}_{mn}}\left[\int_{r=0}^{a}\int_{z=0}^{d} \rho_1 c_{p1} g_1(r,z,t) F^{*}_{1,mn}(r,z) r dr dz\right.$$

$$+\int_{r=a}^{b}\int_{z=0}^{d}\rho_2 c_{p2} g_2(r,z,t) F^{*}_{2,mn}(r,z) r dr dz\Bigg]\exp\left(\lambda^{*2}_{mn}\, t\right) \tag{44}$$

$$\frac{dA^{**}_{mn}}{dt} = \frac{1}{N^{**}_{mn}}\Bigg[\int_{r=0}^{a}\int_{z=0}^{d}\rho_1 c_{p1} g_1(r,z,t) F^{**}_{1,mn}(r,z) r dr dz$$

$$+\int_{a}^{b}\int_{0}^{d}\rho_2 c_{p2} g_2(r,z,t) F^{**}_{2,mn}(r,z) r dr dz\Bigg]\exp\left(\lambda^{**2}_{mn}\, t\right) \tag{45}$$

The differential equations (43), (44), and (45) are integrated and substituted into Eqs. (14) and (15). The resultant integration constants are calculated applying the initial conditions (8). The final forms of the functions $A_{mn}(t)$, $A^{*}_{mn}(t)$, and $A^{**}_{mn}(t)$ are

$$A_{mn}(t) = \Lambda_{mn} + \frac{1}{N_{mn}}\int_{\tau=0}^{t}\Bigg[\int_{r=0}^{a}\int_{z=0}^{d}\rho_1 c_{p1} g_1(r,z,\tau) F_{1,mn}(r,z) r dr dz$$

$$+\int_{r=a}^{b}\int_{z=0}^{d}\rho_2 c_{p2} g_2(r,z,\tau) F_{2,mn}(r,z) r dr dz\Bigg]\exp\left(\lambda^{2}_{mn}\,\tau\right) d\tau \tag{46}$$

$$A^{*}_{mn}(t) = \Lambda^{*}_{mn} + \frac{1}{N^{*}_{mn}}\int_{\tau=0}^{t}\Bigg[\int_{r=0}^{a}\int_{z=0}^{d}\rho_1 c_{p1} g_1(r,z,\tau) F^{*}_{1,mn}(r,z) r dr dz$$

$$+\int_{r=a}^{b}\int_{z=0}^{d}\rho_2 c_{p2} g_2(r,z,\tau) F^{*}_{2,mn}(r,z) r dr dz\Bigg]\exp\left(\lambda^{*2}_{mn}\,\tau\right) d\tau \tag{47}$$

$$A^{**}_{mn}(t) = \Lambda^{**}_{mn} + \frac{1}{N^{**}_{mn}}\int_{\tau=0}^{t}\Bigg[\int_{r=0}^{a}\int_{z=0}^{d}\rho_1 c_{p1} g_1(r,z,\tau) F^{**}_{1,mn}(r,z) r dr dz$$

$$+\int_{r=a}^{b}\int_{z=0}^{d}\rho_2 c_{p2} g_2(r,z,\tau) F^{**}_{2,mn}(r,z) r dr dz\Bigg]\exp\left(\lambda^{**2}_{mn}\,\tau\right) d\tau \tag{48}$$

where the integration constants Λ_{mn}, Λ^{*}_{mn}, and Λ^{**}_{mn} are given by

$$\Lambda_{mn} = \frac{1}{N_{mn}}\Bigg[\int_{r=0}^{a}\int_{z=0}^{d}\rho_1 c_{p1} f_1(r,z) F_{1,mn}(r,z) r dr dz$$

$$+\int_{r=a}^{b}\int_{z=0}^{d}\rho_2 c_{p2} f_2(r,z) F_{2,mn}(r,z) r dr dz\Bigg] \tag{49}$$

$$\Lambda^{*}_{mn} = \frac{1}{N^{*}_{mn}}\Bigg[\int_{r=0}^{a}\int_{z=0}^{d}\rho_1 c_{p1} f_1(r,z) F^{*}_{1,mn}(r,z) r dr dz$$

$$+\int_{r=a}^{b}\int_{z=0}^{d}\rho_2 c_{p2} f_2(r,z) F^{*}_{2,mn}(r,z) r dr dz\Bigg] \tag{50}$$

$$\Lambda_{mn}^{**}=\frac{1}{N_{mn}^{**}}\left[\int_{r=0}^{a}\int_{z=0}^{d}\rho_1 c_{p1} f_1(r,z)F_{1,mn}^{**}(r,z)rdrdz + \int_{r=a}^{b}\int_{z=0}^{d}\rho_2 c_{p2} f_2(r,z)F_{2,mn}^{**}(r,z)rdrdz\right] \tag{51}$$

Equations (46) through (51) provide explicit expressions for the functions $A_{mn}(t)$, $A_{mn}^{*}(t)$, and $A_{mn}^{**}(t)$ that should be used in the construction of the temperature solutions given by Eqs. (14) and (15). The eigenvalues calculated using Eqs. (34) and (35) or Eqs. (34) and (36) apply for a solution with a prescribed heat flux at the surface $r=b$. This is the case of Eq. (7). If a solution with a different boundary condition at the surface $r=b$ is needed, the transcendental equations (34), (35), and (36) need to be modified. For example, for a prescribed temperature at the surface $r=b$, Eq.(9) yields the following transcendental equations

$$C_{mn}/D_{mn}=-Y_0(\gamma_{mn}\bar{b})/J_0(\gamma_{mn}\bar{b}) \quad \text{for } \alpha_1<\alpha_{z2} \text{ or } \alpha_1>\alpha_{z2} \tag{52}$$

$$C_{mn}^{*}/D_{mn}^{*}=-K_0(\gamma_{mn}^{*}\bar{b})/I_0(\gamma_{mn}^{*}\bar{b}) \quad \text{for } \alpha_1<\alpha_{z2} \tag{53}$$

$$C_{mn}^{**}/D_{mn}^{**}=-Y_0(\gamma_{mn}^{**}\bar{b})/J_0(\gamma_{mn}^{**}\bar{b}) \quad \text{for } \alpha_1>\alpha_{z2} \tag{54}$$

It is pointed out that Eqs. (14) through (33) and Eqs. (46) through (51) can still be used to construct the solution for a prescribed temperature at the surface $r=b$. The only difference arises in the calculation of the eigenvalues which is carried out using Eqs. (52) and (53) or Eqs. (52) and (54). A convective boundary condition at the surface $r=b$ requires that

$$-k_{r2}\frac{\partial T_2}{\partial r}+hT_2=hT_\infty \quad \text{at } r=b \text{ in } 0<z<d \tag{55}$$

where h is the heat transfer coefficient and T_∞ is the temperature of the environment. Equation (55) produces the following transcendental equations

$$\begin{aligned}&-k_{r2}\,k\,\gamma_{mn}\left[C_{mn}J_1(\gamma_{mn}\bar{b})+D_{mn}Y_1(\gamma_{mn}\bar{b})\right]=\\ &-h\left[C_{mn}J_0(\gamma_{mn}\bar{b})+D_{mn}Y_0(\gamma_{mn}\bar{b})\right] \quad \text{for } \alpha_1<\alpha_{z2} \text{ or } \alpha_1>\alpha_{z2}\\ &-k_{r2}\,k\,\gamma_{mn}^{*}\left[C_{mn}^{*}I_1(\gamma_{mn}^{*}\bar{b})-D_{mn}^{*}K_1(\gamma_{mn}^{*}\bar{b})\right]=\end{aligned} \tag{56}$$

$$-h\left[C^{*}_{mn}I_0(\gamma^{*}_{mn}\bar{b})+D^{*}_{mn}K_0(\gamma^{*}_{mn}\bar{b})\right] \text{ for } \alpha_1<\alpha_{z2} \tag{57}$$

$$-k_{r2}\,k\,\gamma^{**}_{mn}\left[C^{**}_{mn}J_1(\gamma^{**}_{mn}\bar{b})+D^{**}_{mn}Y_1(\gamma^{**}_{mn}\bar{b})\right]=$$

$$-h\left[C^{**}_{mn}J_0(\gamma^{**}_{mn}\bar{b})+D^{**}_{mn}Y_0(\gamma^{**}_{mn}\bar{b})\right] \text{ for } \alpha_1>\alpha_{z2} \tag{58}$$

Once the eigenvalues from Eqs. (56) and (57) or Eqs. (56) and (58) are calculated, the solution for this convective boundary condition can be constructed using Eqs. (14)-(33) and Eqs. (46)-(51). It can be seen from the transcendental equations (56)-(58) that the computation of the eigenvalues for the convective case becomes more demanding.

Thermal Equilibrium Prediction

Parametric studies for the prediction of thermal equilibrium can be carried out using the temperature solutions, Eqs. (14) and (15), and an appropriate boundary condition. The selection of the boundary condition depends on the particular application. For example, if the calorimeter is releasing heat to an environment at a temperature T_∞, a convective boundary condition, Eq. (55), is more appropriate. When the outer surface of the calorimeter is maintained at a constant temperature by means of a temperature control system, a boundary condition of the first kind, Eq. (9), is a better choice. The prescribed heat flux boundary condition, Eq. (7), is useful to estimate the time required for thermal equilibrium when a specified amount of heat is being extracted at the surface $r=b$. This boundary condition is useful in design calculations to determine an appropriate choice for a temperature control system. Simulations for prescribed temperature and heat flux boundary conditions are presented in this paper. The inner cylinder in these simulations is composed of PuO_2 powder. Effective properties are used in this case (R.G. Deissler and C. S. Eian, 1952), and they include the effects of the porosity and fill gas of the plutonium oxide powder. The thermal equilibrium predictions are carried out assuming that the PuO_2 powder is filled with air. The thermal properties of the outer cylindrical

layer are taken as generic. The experimental estimation of the thermophysical properties of the inner cylinder and the outer cylindrical layer is a subject for future research.

Thermal Equilibrium for a Prescribed Heat Flux at the Surface *r=b*. It is assumed that there is a constant volumetric heat generation, g_0, due to nuclear reactions in the inner cylinder. When thermal equilibrium is reached in the calorimeter, the temperature at any point should not change with time. This is known as a steady-state condition. In order to achieve a steady-state condition, the energy released by the PuO_2 powder should be equal to the energy transferred at the surface $r = b$. This is the case where there are no heat losses at the surfaces $z = 0$ and $z = d$. When there are heat losses at the surfaces $z = 0$ and $z = d$, a steady-state condition can be achieved if the energy released in the inner cylinder, $g_0 V_0$, is equal to the sum of the energy losses through the surfaces $r = b$, $z = 0$, and $z = d$.

An algorithm for the computation of the eigenvalues for the prescribed heat flux at $r = b$ case was developed prior to the construction of the solution given by Eqs. (14) and (15). The computer program that constructs this solution was written in FORTRAN. The efficient and fast computation of the eigenvalues needs special attention. Due to the nature of the transcendental equations (34)-(36), a large number of eigenvlaues may be contained in a small interval and consequently, an algorithm that makes sure that all the eigenvalues are included in the construction of the solution is essential. The algorithm for the calculation of the eigenvalues is not discussed here because of space limitations. With the purpose of verifying the implementation of the FORTRAN program and carrying out preliminary thermal equilibrium predictions, it is assumed that the heat flux functions on the right-sides of Eqs.(4) and (5) are constants, that is

$$k_1 \frac{\partial T_1}{\partial z} = q_{z1} = \text{constant} \quad \text{at} \quad z = 0 \ \text{in} \ 0 < r < a \tag{59}$$

$$k_1 \frac{\partial T_1}{\partial z} = q_{z2} = \text{constant} \quad \text{at} \quad z = d \ \text{in} \ 0 < r < a \tag{60}$$

Furthermore, the boundary condition (7) is assumed to be constant

$$k_{r2}\frac{\partial T_2}{\partial r} = q_0 = \text{constant at } r = b \text{ in } 0 < z < d \tag{61}$$

The construction of this solution is done using Eqs. (59)-(61), (14)-(33), and (46)-(51) to obtain

$$T_i(r,z,t) = \frac{g_0 F_{i,00} a^2 d}{2N_{00}} t - \frac{q_0 F_{i,00} bd}{N_{00}} t - \frac{q_{z2} F_{i,00} a^2}{2N_{00}} t - \frac{q_{z1} F_{i,00} a^2}{2N_{00}} t$$

$$+ g_0 d \sum_{m=1}^{\infty} \frac{F_{i,m0}(r,z) a J_1(\eta_{m0} a)}{\eta_{m0} \lambda_{m0}^2 N_{m0}} \left[1 - \exp(-\lambda_{m0}^2 t)\right]$$

$$- q_0 db \sum_{m=1}^{\infty} \frac{F_{i,m0}(r,z)}{\lambda_{m0}^2 N_{m0}} \left[C_{m0} J_0(\gamma_{m0} \bar{b}) + D_{m0} Y_0(\gamma_{m0} \bar{b})\right] \left[1 - \exp(-\lambda_{m0}^2 t)\right]$$

$$- a \sum_{m=1}^{\infty} \sum_{n=0}^{\infty} \frac{F_{i,mn}(r,z) J_1(\eta_{mn} a)}{\lambda_{mn}^2 N_{mn} \eta_{mn}} \left[q_{z1} + q_{z2} \cos(n\pi)\right] \left[1 - \exp(-\lambda_{mn}^2 t)\right]$$

$$- a \sum_{m=1}^{\xi(n)} \sum_{n=1}^{\infty} \frac{F_{i,mn}^{**}(r,z) I_1(\eta_{mn}^{**} a)}{\lambda_{mn}^{**2} N_{mn}^{**} \eta_{mn}^{**}} \left[q_{z1} + q_{z2} \cos(n\pi)\right] \left[1 - \exp(-\lambda_{mn}^{**2} t)\right] \text{ for } \alpha_1 > \alpha_{z2} \tag{62}$$

where $i = 1,2$. For the case when $\alpha_1 < \alpha_{z2}$ this solution has the form

$$T_i(r,z,t) = \frac{g_0 F_{i,00} a^2 d}{2N_{00}} t - \frac{q_0 F_{i,00} bd}{N_{00}} t - \frac{q_{z2} F_{i,00} a^2}{2N_{00}} t - \frac{q_{z1} F_{i,00} a^2}{2N_{00}} t$$

$$+ g_0 d \sum_{m=1}^{\infty} \frac{F_{i,m0}(r,z) a J_1(\eta_{m0} a)}{\eta_{m0} \lambda_{m0}^2 N_{m0}} \left[1 - \exp(-\lambda_{m0}^2 t)\right]$$

$$- q_0 db \sum_{m=1}^{\infty} \frac{F_{i,m0}(r,z)}{\lambda_{m0}^2 N_{m0}} \left[C_{m0} J_0(\gamma_{m0} \bar{b}) + D_{m0} Y_0(\gamma_{m0} \bar{b})\right] \left[1 - \exp(-\lambda_{m0}^2 t)\right]$$

$$- a \sum_{m=1}^{\infty} \sum_{n=0}^{\infty} \frac{F_{i,mn}(r,z) J_1(\eta_{mn} a)}{\lambda_{mn}^2 N_{mn} \eta_{mn}} \left[q_{z1} + q_{z2} \cos(n\pi)\right] \left[1 - \exp(-\lambda_{mn}^2 t)\right]$$

$$- a \sum_{m=1}^{\xi(n)} \sum_{n=1}^{\infty} \frac{F_{i,mn}^{*}(r,z) J_1(\eta_{mn}^{*} a)}{\lambda_{mn}^{*2} N_{mn}^{*} \eta_{mn}^{*}} \left[q_{z1} + q_{z2} \cos(n\pi)\right] \left[1 - \exp(-\lambda_{mn}^{*2} t)\right]$$

$$\text{for } i = 1,2 \text{ and } \alpha_1 < \alpha_{z2} \tag{63}$$

Notice that Eqs. (62) and (63) differ on the last summation term. Thermal equilibrium with the environment is attained when the accumulation of energy in the two-domain cylinder is equal to zero. This condition is satisfied if

$$g_0 V_0 - q_0 A_0 - q_{z1} A_d - q_{z2} A_d = 0 \tag{64}$$

where V_0 is the volume of the inner cylinder, $A_0 = 2\pi bd$ is the lateral area of the outer cylinder, and $A_d = \pi a^2$ is the area of the top or bottom surface of the inner cylinder. It is assumed that there are no heat losses through the top and bottom surfaces of the outer cylindrical layer. This assumption is made to make the presentation of the procedure more compact. Furthermore, in practice the top and bottom surfaces of a calorimeter are well insulated and heat losses through these surfaces are neglected.

A solution that reaches steady-state conditions as $t \to \infty$ can be obtained from Eqs. (62) and (63) by requiring that each one of the energies transferred through the surfaces $r = b$, $z = 0$, and $z = d$ is equal to a fraction of the energy released in the inner cylinder. This leads to the following definitions

$$q_0 A_0 = x_0 g_0 V_0, \; q_{z1} A_d = x_{z1} g_0 V_0, \text{ and } q_{z2} A_d = x_{z2} g_0 V_0 \tag{65}$$

with the requirement that

$$x_0 + x_{z1} + x_{z2} = 1 \tag{66}$$

Note that Eq. (66) ensures the satisfaction of Eq. (64) which requires that there is no accumulation of energy in the calorimeter. If $x_{z1} = x_{z2}$, the resultant temperature distribution given by Eqs. (62) and (63) is symmetric with respect to the plane $z = d/2$. This symmetry condition is convenient to verify the numerical output of the FORTRAN program used to implement Eqs. (62) and (63). This verification was done checking the symmetry and comparing the numerical output of Eqs. (62) and (63) with a finite elements implementation of the solution. The thermal equilibrium prediction can be implemented using Eqs. (65) and (66). The assumption, $x_{z1} = x_{z2}$, and Eqs. (65) lead to

$$q_0 = \frac{x_0 g_0 a^2}{2b}, \; q_{z1} = q_{z2} = x_{z1} g_0 d \tag{67}$$

Furthermore, substituting the definitions of the heat fluxes given by Eq. (67) into the terms that multiply time, t, in Eqs. (62) and (63) yields

$$\left[\frac{g_0 F_{i,00} a^2 d}{2N_{00}} - \frac{(x_0 + x_{z1} + x_{z2}) g_0 F_{i,00} a^2 d}{2N_{00}}\right] t = 0 \tag{68}$$

Equations (65) and (68) show that all the terms that multiply the time, t, on the right-side of Eqs. (62) and (63) cancel out when the definitions of the heat fluxes given by Eqs. (67) are used. This is to be expected because Eq. (67) satisfies the energy balance (64). Equations (62), (63), (67), and (68) yield

$$T_i(r,z,t) = g_0 d \sum_{m=1}^{\infty} \frac{F_{i,m0}(r,z) a J_1(\eta_{m0} a)}{\eta_{m0} \lambda_{m0}^2 N_{m0}} \left[1 - \exp(-\lambda_{m0}^2 t)\right]$$

$$- \frac{x_0 g_0 a^2 d}{2} \sum_{m=1}^{\infty} \frac{F_{i,m0}(r,z)}{\lambda_{m0}^2 N_{m0}} \left[C_{m0} J_0(\gamma_{m0} \bar{b}) + D_{m0} Y_0(\gamma_{m0} \bar{b})\right] \left[1 - \exp(-\lambda_{m0}^2 t)\right]$$

$$- x_{z1} g_0 a d \sum_{m=1}^{\infty} \sum_{n=0}^{\infty} \frac{F_{i,mn}(r,z) J_1(\eta_{mn} a)}{\lambda_{mn}^2 N_{mn} \eta_{mn}} \left[1 + \cos(n\pi)\right] \left[1 - \exp(-\lambda_{mn}^2 t)\right]$$

$$- x_{z1} g_0 a d \sum_{m=1}^{\xi(n)} \sum_{n=1}^{\infty} \frac{F^*_{i,mn}(r,z) J_1(\eta^*_{mn} a)}{\lambda^{*2}_{mn} N^*_{mn} \eta^*_{mn}} \left[1 + \cos(n\pi)\right] \left[1 - \exp(-\lambda^{*2}_{mn} t)\right]$$

$$\text{for } i = 1,2 \text{ and } \alpha_1 < \alpha_{z2} \tag{69}$$

$$T_i(r,z,t) = g_0 d \sum_{m=1}^{\infty} \frac{F_{i,m0}(r,z) a J_1(\eta_{m0} a)}{\eta_{m0} \lambda_{m0}^2 N_{m0}} \left[1 - \exp(-\lambda_{m0}^2 t)\right]$$

$$- \frac{x_0 g_0 a^2 d}{2} \sum_{m=1}^{\infty} \frac{F_{i,m0}(r,z)}{\lambda_{m0}^2 N_{m0}} \left[C_{m0} J_0(\gamma_{m0} \bar{b}) + D_{m0} Y_0(\gamma_{m0} \bar{b})\right] \left[1 - \exp(-\lambda_{m0}^2 t)\right]$$

$$- x_{z1} g_0 a d \sum_{m=1}^{\infty} \sum_{n=0}^{\infty} \frac{F_{i,mn}(r,z) J_1(\eta_{mn} a)}{\lambda_{mn}^2 N_{mn} \eta_{mn}} \left[1 + \cos(n\pi)\right] \left[1 - \exp(-\lambda_{mn}^2 t)\right]$$

$$- x_{z1} g_0 a d \sum_{m=1}^{\xi(n)} \sum_{n=1}^{\infty} \frac{F^{**}_{i,mn}(r,z) I_1(\eta^{**}_{mn} a)}{\lambda^{**2}_{mn} N^{**}_{mn} \eta^{**}_{mn}} \left[1 + \cos(n\pi)\right] \left[1 - \exp(-\lambda^{**2}_{mn} t)\right]$$

$$\text{for } i = 1,2 \text{ and } \alpha_1 > \alpha_{z2} \tag{70}$$

An estimation of the time required to reach thermal equilibrium can be obtained using Eqs. (69) or (70). Note that as $t \to \infty$, the exponential terms in Eqs. (69) and (70) tend to zero and limiting solutions independent of time are obtained. Preliminary calculations are carried out using Eq. (69) assuming that the inner cylindrical region is filled with PuO_2 powder with the following thermophysical properties: $k_1 = 0.00243\ W/(cm\ ^\circ C)$ and $\rho_1 c_{p1} = 1.28\ J/(cm^3\ ^\circ C)$. These properties correspond to a porosity of 0.415. The porosity is defined as the volume occupied by the fill gas over the total volume. The fill gas is assumed to be air. The dimensions of the inner and outer cylinders are taken as: $a = 5.65\ cm$, $b = 9.74\ cm$, and $d = 11.0\ cm$. The dimensions of the inner cylinder correspond to a mass of $5\ kg$ of plutonium oxide powder. A power density of $3.00601202\ W/kg$ (T.D. Knight and R.G. Steinke, 1997) is assumed to calculate the volumetric heat generation, g_0. The thermal properties of the outer cylinder are taken as: $k_{r2} = 3.7\ W/(cm\ ^\circ C)$, $k_{z2} = 0.8\ W/(cm\ ^\circ C)$, and $\rho_2 c_{p2} = 3.037\ J/(cm^3\ ^\circ C)$. Constant initial conditions equal to $25\ ^\circ C$ are used to carry out these simulations. The variation of temperature with respect to the radius at $z = d/2$ is shown in Fig. 2. Figure 2 also shows the temperature curves for different values of time up to the time when thermal equilibrium is reached. It is seen from Fig. 2 that thermal equilibrium is reached when time is equal to 28360 seconds. This time corresponds to 7.88 hours. It is assumed that thermal equilibrium is reached when there is no significant change in temperature with time at any location of the two-domain cylinder. For this case the temperature at the center of the cylinder is used as: $|T_1(0, d/2, 28360) - T_1(0, d/2, 27360)| = 3.15 \times 10^{-4}\ ^\circ C$. For the set of thermophysical properties mentioned earlier, the smallest eigenvalue in Eq. (69) is $\lambda_{1,0} = 3.25376 \times 10^{-3}\ s^{-1/2}$. Notice that $\exp[-(3.25376 \times 10^{-3})^2\ s^{-1}\ 28360\ s] \sim 1$ which indicates that all the exponential terms in Eq. (69) are close to zero when $t = 28360\ s$. Furthermore, when the exponential terms are zero, Eq. (69) becomes

independent of time. The values of x_0, x_{z1}, and x_{z2} used in these simulations are: $x_0 = 0.93$, $x_{z1} = x_{z2} = 0.035$.

It has been verified from calorimetric measurements that the variation of the heat flux at the surface $r = b$ can be expressed in terms of exponentials (C. L. Fellers and P.W. Seabaugh, 1979; M. K. Smith and D. S. Bracken, 2000)

$$q(t) = A + \sum_{\nu=1}^{P} B_{2\nu-1} \exp(-\varphi_{2\nu} t) \tag{71}$$

The constants in Eq. (71) are estimated using experimental power measurements and a nonlinear least-squares procedure. Equation (71) can be used to implement an energy balance similar to Eq. (64). However, when Eq. (71) is used, the energy balance is satisfied in the limit as $t \to \infty$. It is pointed out that a constant heat flux output form the outer surface of the calorimeter since the beginning of an experiment would be difficult to implement in the laboratory. Boundary condition (61) was selected to verify the program and carry out preliminary equilibrium predictions. A more realistic boundary condition is to maintain the outer surface of the calorimeter at a constant temperature. This corresponds to boundary condition (9). Note from Fig. 2 that the temperature in the outer cylindrical layer is nearly constant. The value of this temperature can be used to make a more realistic thermal equilibrium prediction using boundary condition (9). Typically, the temperature of the outer surface of a calorimeter is maintained constant using a temperature control system.

Thermal Equilibrium for a Prescribed Temperature at the Surface *r=b*. A temperature solution is developed using the same thermophysical properties and initial conditions used in the prescribed heat flux case. Boundary conditions (59) and (60) are also used to construct this solution. The only difference here is the boundary condition at $r = b$ which is taken as

$$T_2(b, z, t) = T_s = \text{constant in } 0 < z < d \tag{72}$$

Since the eigenfunctions used in the construction of the solution that should satisfy boundary condition (72) vanish at the surface $r=b$, the solution converges poorly near or at the surface $r=b$. In order to alleviate this difficulty, a simple temperature transformation is defined as

$$\theta_i(r,z,t)=T_i(r,z,t)-T_s \quad \text{for } i=1,2 \tag{73}$$

Equation (73) transforms Eqs. (1)-(5), (7)-(8), and (72) into

$$k_1\frac{1}{r}\frac{\partial}{\partial r}\left(r\frac{\partial\theta_1}{\partial r}\right)+k_1\frac{\partial^2\theta_1}{\partial z^2}+g_1(r,z,t)=\rho_1 c_{p1}\frac{\partial\theta_1}{\partial t} \quad \text{in } 0<r<a \tag{74}$$

$$k_{r2}\frac{1}{r}\frac{\partial}{\partial r}\left(r\frac{\partial\theta_2}{\partial r}\right)+k_{z2}\frac{\partial^2\theta_2}{\partial z^2}+g_2(r,z,t)=\rho_2 c_{p2}\frac{\partial\theta_2}{\partial t} \quad \text{in } a<r<b \tag{75}$$

$$\frac{\partial\theta_1}{\partial r}=0 \quad \text{at} \quad r=0 \tag{76}$$

$$k_1\frac{\partial\theta_1}{\partial z}=q_{z1}(r,t) \quad \text{at } z=0 \text{ in } 0<r<a \tag{77}$$

$$k_1\frac{\partial\theta_1}{\partial z}=q_{z2}(r,t) \quad \text{at } z=d \text{ in } 0<r<a \tag{78}$$

$$k_{z2}\frac{\partial\theta_2}{\partial z}=0 \quad \text{at } z=0 \text{ and } z=d \text{ in } a<r<b \tag{79}$$

$$\theta_2(b,z,t)=0 \text{ in } 0<z<d \tag{80}$$

$$\theta_1(r,z,0)=f_1^*(r,z) \text{ and } \theta_2(r,z,0)=f_2^*(r,z) \tag{82}$$

The solution obtained from Eqs. (74)-(82) satisfies boundary condition (72) and has good convergence behavior close to the surface $r=b$. The construction of this solution is done using Eqs. (76)-(82), (14)-(33), and (46)-(51). Notice that when using Eqs. (14)-(33) and (46)-(51) T_i should be replaced by θ_i for $i=1,2$. The resultant solution has the form

$$T_i(r,z,t)=T_s+g_0 d\sum_{m=1}^{\infty}\frac{F_{i,m0}(r,z)a\,J_1(\eta_{m0}a)}{\eta_{m0}\,\lambda_{m0}^2 N_{m0}}\left[1-\exp(-\lambda_{m0}^2 t)\right]$$

$$+\rho_1 c_{p1}(T_{0,1}-T_s)\sum_{m=1}^{\infty}\frac{F_{i,m0}(r,z)\exp(-\lambda_{m0}^2 t)}{N_{m0}}\frac{ad\,J_1(\eta_{m0}a)}{\eta_{m0}}$$

$$+\frac{\rho_2 c_{p2}(T_{0,2}-T_s)\sqrt{k_{r2}}}{\sqrt{k_{z2}}}\sum_{m=1}^{\infty}\frac{d\,F_{i,m0}(r,z)\exp(-\lambda_{m0}^2 t)}{\gamma_{m0}N_{m0}}\left\{C_{m0}\left[bJ_1(\gamma_{m0}\bar{b})-aJ_1(\gamma_{m0}\bar{a})\right]\right.$$

$$+ D_{m0}\left[bY_1(\gamma_{m0}\bar{b}) - aY_1(\gamma_{m0}\bar{a})\right]\Big\}$$

$$-a\sum_{m=1}^{\infty}\sum_{n=0}^{\infty}\frac{F_{i,mn}(r,z)J_1(\eta_{mn}a)}{\lambda_{mn}^2 N_{mn}\eta_{mn}}\left[q_{z1}+q_{z2}\cos(n\pi)\right]\left[1-\exp(-\lambda_{mn}^2 t)\right]$$

$$-a\sum_{m=1}^{\xi(n)}\sum_{n=1}^{\infty}\frac{F^{*}_{i,mn}(r,z)J_1(\eta^{*}_{mn}a)}{\lambda^{*2}_{mn}N^{*}_{mn}\eta^{*}_{mn}}\left[q_{z1}+q_{z2}\cos(n\pi)\right]\left[1-\exp(-\lambda^{*2}_{mn}t)\right]$$

$$\text{for } i=1,2 \text{ and } \alpha_1 < \alpha_{z2} \tag{83}$$

where $T_{0,1}$ and $T_{0,2}$ are the initial conditions in the inner and outer cylindrical layers respectively. These initial conditions are assumed to be constants. The solution that applies when $\alpha_1 > \alpha_{z2}$ is given by

$$T_i(r,z,t) = T_s + g_0 d\sum_{m=1}^{\infty}\frac{F_{i,m0}(r,z)a\,J_1(\eta_{m0}a)}{\eta_{m0}\,\lambda_{m0}^2 N_{m0}}\left[1-\exp(-\lambda_{m0}^2 t)\right]$$

$$+\rho_1 c_{p1}(T_{0,1}-T_s)\sum_{m=1}^{\infty}\frac{F_{i,m0}(r,z)\exp(-\lambda_{m0}^2 t)}{N_{m0}}\frac{ad\,J_1(\eta_{m0}a)}{\eta_{m0}}$$

$$+\frac{\rho_2 c_{p2}(T_{0,2}-T_s)\sqrt{k_{r2}}}{\sqrt{k_{z2}}}\sum_{m=1}^{\infty}\frac{d\,F_{i,m0}(r,z)\exp(-\lambda_{m0}^2 t)}{\gamma_{m0}N_{m0}}\Big\{C_{m0}\left[bJ_1(\gamma_{m0}\bar{b}) - aJ_1(\gamma_{m0}\bar{a})\right]$$

$$+ D_{m0}\left[bY_1(\gamma_{m0}\bar{b}) - aY_1(\gamma_{m0}\bar{a})\right]\Big\}$$

$$-a\sum_{m=1}^{\infty}\sum_{n=0}^{\infty}\frac{F_{i,mn}(r,z)J_1(\eta_{mn}a)}{\lambda_{mn}^2 N_{mn}\eta_{mn}}\left[q_{z1}+q_{z2}\cos(n\pi)\right]\left[1-\exp(-\lambda_{mn}^2 t)\right]$$

$$-a\sum_{m=1}^{\xi(n)}\sum_{n=1}^{\infty}\frac{F^{**}_{i,mn}(r,z)I_1(\eta^{**}_{mn}a)}{\lambda^{**2}_{mn}N^{**}_{mn}\eta^{**}_{mn}}\left[q_{z1}+q_{z2}\cos(n\pi)\right]\left[1-\exp(-\lambda^{**2}_{mn}t)\right]$$

$$\text{for } i=1,2 \text{ and } \alpha_1 > \alpha_{z2} \tag{84}$$

Equations (83) and (84) become independent of time in the limit as $t \to \infty$. A more realistic estimation of the time required for equilibrium can be obtained from Eqs. (83) or (84). The surface temperature, T_s, is assumed to be close to the surface temperatures shown in Fig. 2. These surface temperatures were obtained from the Eq. (69). It is

expected that the prescribed temperature thermal equilibrium model will predict a larger equilibrium time because it contains the effects of the summation terms of Eq. (71). It is assumed that the surface temperature, T_s, is maintained at 21.321417 $^{\circ}C$. The variation of temperature with respect to the radius at $z = d/2$ generated by the prescribed temperature model is shown in Fig. 3. Figure 3 also shows the temperature curves for different values of time up to the time when thermal equilibrium is reached. It is seen from Fig. 3 that thermal equilibrium is reached when time is equal to 32360 seconds. This time corresponds to 8.99 hours. A criterion for thermal equilibrium that has the same order of magnitude than the criterion used for the prescribed heat flux model is used here. Also, the temperature at the center of the inner cylindrical region is used as an equilibrium criterion as: $\left|T_1(0,d/2,32360) - T_1(0,d/2,31360)\right| = 2.804\times10^{-4}$ $^{\circ}C$. The use of the same thermal equilibrium criterion provides a basis for comparison between the two models. The prescribed temperature model predicts thermal equilibrium 1.11 hours later than the prescribed heat flux model. The prescribed temperature model prediction is considered to be closer to experimental conditions. However, note that a surface temperature obtained from the prescribed heat flux model was used to start the calculations with the prescribed temperature model. The fact that the prescribed temperature model contains the effects of the summation terms on the right-hand side of Eq. (71) can be seen by differentiating Eq. (83) with respect to the radius to obtain the heat flux at the surface $r = b$

$$-k_{r2}\left.\frac{\partial T_2}{\partial r}\right|_{r=b} = -k_{r2}\, g_0 d \sum_{m=1}^{\infty} \left.\frac{a\, J_1(\eta_{m0}a)}{\eta_{m0}\,\lambda_{m0}^2 N_{m0}} \frac{\partial F_{2,m0}}{\partial r}\right|_{r=b} \left[1-\exp(-\lambda_{m0}^2 t)\right]$$

$$-k_{r2}\rho_1 c_{p1}(T_{0,1}-T_s)\sum_{m=1}^{\infty} \left.\frac{\exp(-\lambda_{m0}^2 t)}{N_{m0}} \frac{ad\, J_1(\eta_{m0}a)}{\eta_{m0}} \frac{\partial F_{2,m0}}{\partial r}\right|_{r=b}$$

$$-\frac{\rho_2 c_{p2}(T_{0,2}-T_s)k_{r2}^{3/2}}{\sqrt{k_{z2}}} \sum_{m=1}^{\infty} \left.\frac{d\exp(-\lambda_{m0}^2 t)}{\gamma_{m0} N_{m0}} \frac{\partial F_{2,m0}}{\partial r}\right|_{r=b} \left\{C_{m0}\left[bJ_1(\gamma_{m0}\bar{b}) - aJ_1(\gamma_{m0}\bar{a})\right]\right.$$

$$+ D_{m0}\left[bY_1(\gamma_{m0}\bar{b}) - aY_1(\gamma_{m0}\bar{a})\right]\Big\}$$

$$+ k_{r2}a\sum_{m=1}^{\infty}\sum_{n=0}^{\infty}\frac{J_1(\eta_{mn}a)}{\lambda_{mn}^2 N_{mn}\eta_{mn}}\left.\frac{\partial F_{2,mn}}{\partial r}\right|_{r=b}\left[q_{z1}+q_{z2}\cos(n\pi)\right]\left[1-\exp(-\lambda_{mn}^2 t)\right]$$

$$+ k_{r2}a\sum_{m=1}^{\xi(n)}\sum_{n=1}^{\infty}\frac{J_1(\eta_{mn}^*a)}{\lambda_{mn}^{*2} N_{mn}^*\eta_{mn}^*}\left.\frac{\partial F_{2,mn}^*}{\partial r}\right|_{r=b}\left[q_{z1}+q_{z2}\cos(n\pi)\right]\left[1-\exp(-\lambda_{mn}^{*2} t)\right]$$

for $\alpha_1 < \alpha_{z2}$ (85)

Equation (85) is used to obtain the variation of the heat flux with time at $z = d/2$. Data points are generated in the interval $3.236\,s \le t \le 32360\,s$. The early transients are not generated because they have little influence on the onset of thermal equilibrium, which occurs at larger times. Equation (71) is slightly modified to conform with the squared eigenvalues that appear in the arguments of the exponential functions in Eq. (85)

$$q(t) = A + \sum_{\nu=1}^{P} B_{2\nu-1}\exp(-\varphi_{2\nu}^2 t) \tag{86}$$

The data set generated by Eq. (85), and Eq.(86) are used with a nonlinear least-squares procedure to obtain the constants $A, B_{2\nu-1}$, and $\varphi_{2\nu}$. The Levenberg-Marquardt algorithm is applied to solve the nonlinear least-squares problem. The variance between the estimated and exact heat fluxes for this nonlinear curve-fit is found to be equal to 1.291×10^{-15}. The value of the upper limit of the summation in Eq. (86), P, is found to be equal to 29 in this minimization. When $P = 29$, a nonlinear least-squares problem that involves 57 variables is solved to obtain the constants in Eq. (86). The graph of the estimated and exact heat fluxes is given in Fig. 4. A graph of the residuals between Eqs. (85) and (86) is also shown in Fig. 5. The fact that the residuals between Eq. (85) and (86) have an order of magnitude of $10^{-9}\,W/cm^2$ for times greater than 4000 seconds suggests that the form of Eq. (86) should be used to carry out calorimetric thermal equilibrium predictions. Figure 5 shows the residuals for times greater or equal than 1778 seconds.

The criterion used for thermal equilibrium in the prescribed temperature model is applied to the heat flux at $r = b$ represented by Eq. (85) to obtain

$$\left| -k_{r2}\frac{\partial T_2}{\partial r}(b, d/2, 32360) - \left[-k_{r2}\frac{\partial T_2}{\partial r}(b, d/2, 31360) \right] \right| = 8.75\times10^{-8} \qquad (87)$$

Equation (87) shows that the order of magnitude of the variation of the heat flux between 32360 and 31360 seconds is $10^{-8}\, W/cm^2$. Equation (86) obtained from the nonlinear least-squares procedure for $P = 29$ can also be used to predict thermal equilibrium as: $|q(32360) - q(31360)| = 8.74\times10^{-8}$. Notice that the difference given by Eq. (87) is very close to the difference given by Eq. (86).

In order to test the thermal equilibrium prediction capabilities of Eq. (86), a new data set is generated using Eq. (85) in the interval $2.236\, s \le t \le 8067.24\, s$. This period represents 25% of the total time required to reach thermal equilibrium. Again, a nonlinear least-squares procedure is applied to Eq. (86) and this new data set. The variance between the estimated and exact heat fluxes for this curve-fit is found to be equal to 1.88×10^{-12}. Furthermore, the value of P is found to be equal to 17. Equation (86) with P=17 is used to predict the onset of thermal equilibrium as: $|q(32360) - q(31360)| = 8.78\times10^{-8}$. Notice that this thermal equilibrium prediction compares very well with the one given by Eq. (87). Furthermore, the percentage error between the heat flux (at thermal equilibrium) predicted by this least-squares function and the exact value is only 0.005%.

Remarks and Conclusions

This study shows that it is possible to carry out thermal equilibrium predictions with sufficient accuracy using the prescribed heat flux or temperature models. Furthermore, the solutions developed here can be used to carry out parametric studies to investigate the effects of the thermophysical properties of the outer cylindrical layer on the performance of calorimeters.

The data sets generated by Eq. (85) are curved fitted by Eq. (86) with excellent accuracy. Furthermore, when Eq. (86) was applied to the data set contained in the interval $2.236\,s \le t \le 8067.24\,s$, it predicted thermal equilibrium time and the heat flux at equilibrium with very good accuracy. This is an encouraging result taking into consideration that this data set represents only 25% of the total time required for thermal equilibrium. However, further research is needed to test Eq. (86) with data sets that contain levels of noise that are usually encountered in calorimetric measurements.

The temperature solutions developed here can be used to solve an interesting class of inverse heat conduction problems. Furthermore, these solutions and experimental data can be used to estimate the thermophysical properties of the outer cylindrical layer. The implementation of the temperature solution for a convective boundary condition at the surface $r = b$ is a subject for future research.

References

R. G. Deissler and C. S. Eian, 1952, "Investigation of Effective Thermal Conductivities of Powders," National Advisory Committee for Aeronautics report NACA-RM E52C05.

C. L. Fellers and P.W. Seabaugh, 1979, "Real-Time Prediction of Calorimeter Equilibrium," *Nuclear Instruments and Methods* 163, 499.

T. D. Knight and G. R. Steinke, 1997, "Thermal Analyses of Plutonium Materials in British Nuclear Fuels, LTD., Containers," Los Alamos National Laboratory report LA-UR-97-1866.

M. K. Smith and D.S. Bracken, 2000, "The Development of a Multi-Exponential Prediction Algorithm for Calorimetry," Los Alamos National Laboratory report LA-UR-00-3005.

FIGURE CAPTIONS

Figure 1. Two-domain cylindrical geometry.

Figure 2. Temperature distribution at $z = d/2$ generated by Eq. (69). The curve for $t = 28360$ seconds corresponds to the onset of thermal equilibrium for this model.

Figure 3. Temperature distribution at $z = d/2$ generated by Eq. (83). The curve for $t = 32360$ seconds corresponds to the onset of thermal equilibrium for this model.

Figure 4. Exact heat flux data generated by Eq. (85), and $q(t)$ given by the least-squares function (86).

Figure 5. Residuals calculated from Eqs. (85) and (86) for the data set in the interval $3.236\,s \le t \le 32360\,s$.

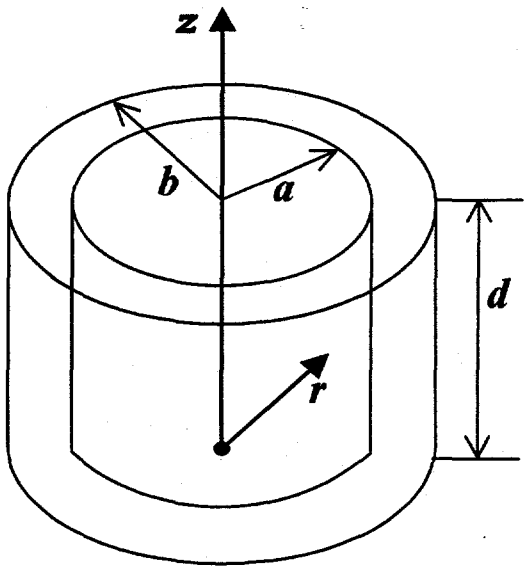

Figure 1. Two-domain cylindrical geometry.

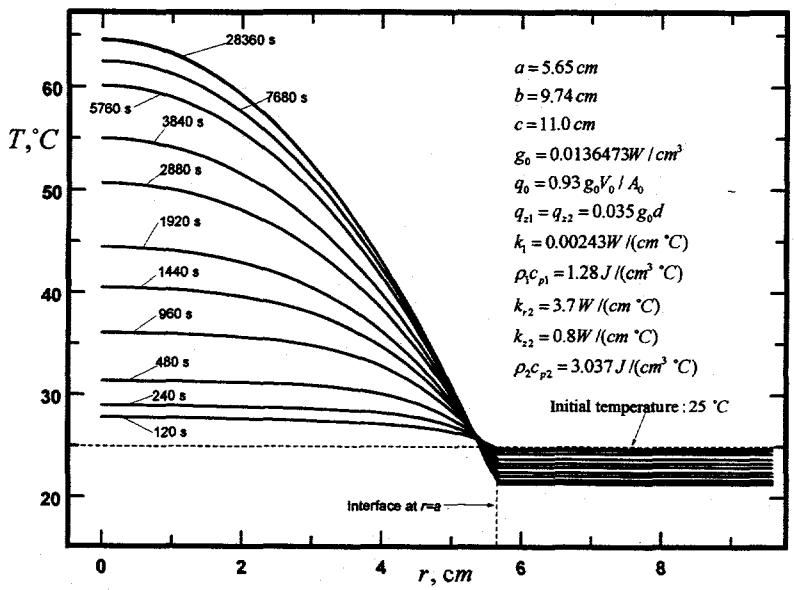

Figure 2. Temperature distribution at $z = d/2$ generated by Eq. (69). The curve for $t = 28360$ seconds corresponds to the onset of thermal equilibrium for this model.

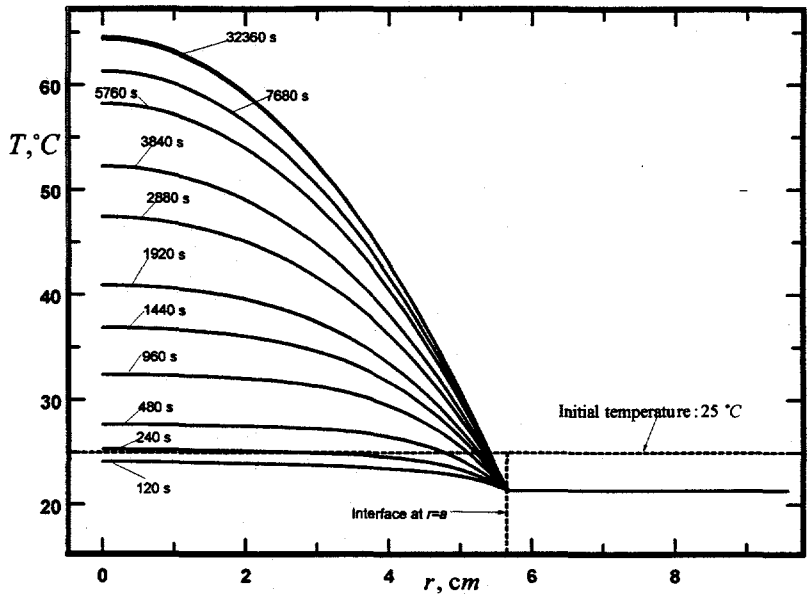

Figure 3. Temperature distribution at $z = d/2$ generated by Eq. (83). The curve for $t = 32360$ seconds corresponds to the onset of thermal equilibrium for this model.

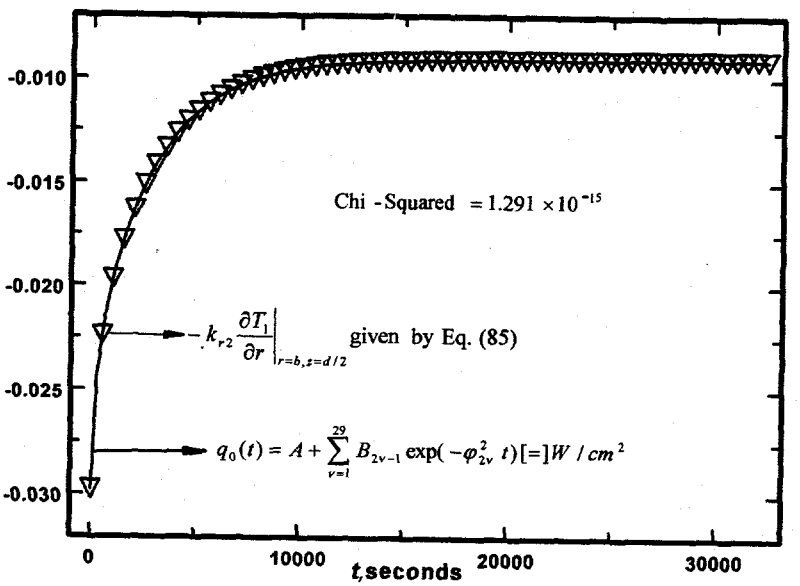

Figure 4. Exact heat flux data generated by Eq. (85), and $q(t)$ given by the least-squares function (86).

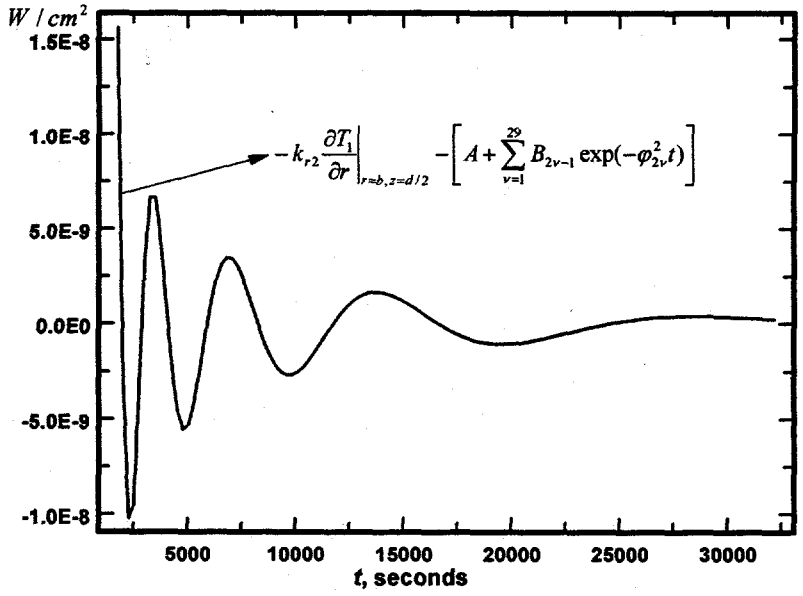

Figure 5. Residuals calculated from Eqs. (85) and (86) for the data set in the interval $3.236\,s \le t \le 32360\,s$.